*Article*

# A Novel Bamboo–Wood Composite Utilizing High-Utilization, Easy-to-Manufacture Bamboo Units: Optimization of Mechanical Properties and Bonding Performance

Yifan Ma [1,2], Yu Luan [1,2], Lin Chen [1,2], Bin Huang [1,2], Xun Luo [1,2], Hu Miao [1,2,*] and Changhua Fang [1,2,*]

1    International Centre for Bamboo and Rattan (ICBR), Beijing 100102, China
2    Key Laboratory of National Forestry and Grassland Administration/Beijing for Bamboo & Rattan Science and Technology, Beijing 100102, China
*    Correspondence: miaohu@icbr.ac.cn (H.M.); cfang@icbr.ac.cn (C.F.)

**Abstract:** Bamboo–wood composites have found extensive applications in the container flooring, furniture, and construction industries. However, commonly utilized bamboo units such as four-side-planed rectangular bamboo strips and bamboo scrimber suffer from either low utilization rates or high adhesive content. The recently developed bamboo-flattening technology, which employs softening methods with saturated high-pressure steam, may improve the utilization rate and reduce the adhesive content, but its complex processes and high cost restrict its widespread application. This study introduces a novel bamboo–wood composite utilizing high-utilization, easy-to-manufacture bamboo units processed through a straightforward flattening-and-grooving method. However, the stress concentration introduced by the grooving treatment may affect the mechanical properties and stability of the bamboo–wood composites. In order to optimize the mechanical properties and bonding performance, response surface methodology based on a central composite rotatable design was used to map the effects of hot-pressing parameters (time, temperature, and pressure) on the mechanical properties. The bamboo-woodbamboo–wood composites prepared with optimized conditions of 1.18 min/mm pressing time, 1.47 MPa pressure, and a 150 °C temperature had a 121.51 MPa modulus of rupture and an 11.85 GPa modulus of elasticity, which exhibited an error of only ~5% between the experimental and model predictions. Finite element analysis revealed that, in comparison to homogeneous flat bamboo composites, grooved bamboo composites exhibited distinct tensile ductility and toughness due to discontinuous stress fields and alternating rigid–soft layers, which alter the stress transmission and energy dissipation mechanisms. Additionally, grooving treatment not only effectively improved the surface wettability of the bamboo plants, thus enhancing the permeability of the adhesive, but also facilitated adhesive penetration into parenchymal cells and fibers. This led to the formation of a more robust glue–nail structure and chemical bonding.

**Keywords:** bamboo; bamboo–wood composite; bamboo-flattening and -grooving unit; response surface methodology; finite element analysis

## 1. Introduction

Bamboo's rapid growth, excellent mechanical properties, and abundant availability position it as an excellent alternative material for wood, which is in short supply [1,2]. Bamboo–wood composites have found extensive applications in container flooring, furniture, and construction [3]. Due to the hollow cylindrical structure of bamboo culms, currently, the most commonly used basic units of bamboo engineering materials are bamboo strips and bamboo scrimber [4]. Bamboo strips are produced by planing arc-shaped bamboo splits on all four sides, resulting in a low material utilization rate (approximately 30%) [5,6]. Bamboo scrimber is manufactured by crushing bamboo splits into bundles, followed by adhesive soaking, drying, and pressing, leading to a higher adhesive content (approximately 15%–30%) [7,8]. These processing steps are numerous and contribute to

high processing costs. Despite recent advancements in bamboo-flattening technology, which have increased the utilization rate and reduced adhesive content to some extent, the method's reliance on high-pressure saturated steam softening leads to complex processes and high costs, thereby limiting its widespread application.

To address the aforementioned challenges, this study introduces a novel bamboo–wood composite with high utilization and simple processing. The process involved the direct and rapid unfolding of arc-shaped bamboo strips, followed immediately by grooving to produce grooved–flattened bamboo (GFB). Both steps were seamlessly executed on the same equipment, ensuring efficiency. Grooving treatment not only enlarges the bonding area but also facilitates adhesive penetration. Subsequent to flattening and grooving, the bamboo fibers and parenchymal cells are fully exposed, leading to enhanced bonding capability. Since it is challenging to apply adhesive directly onto the flattened and grooved bamboo [9], this study employed adhesive application on wooden veneers, significantly enhancing adhesive efficiency. Poplar wood veneers were used in this study for bamboo–wood composite preparation. Due to their low density, they effectively fill the grooves on the bamboo units during hot pressing, enhancing the composite's structural integrity.

However, the stress concentration introduced by the grooving treatment significantly affects the mechanical properties and stability of bamboo–wood composites [10]. Therefore, this study proposes combining the respective advantages of wood and bamboo, utilizing the softer characteristics of wood to solve the stress concentration problem of the grooving process. The fabrication methods of bamboo–wood composites based on the grooved–flattened bamboo (GFB) unit were systematically examined. The material properties were evaluated by assessing the tensile strength and bonding ability of the bamboo-based composites. Initially, mathematical models were developed using response surface methodology (RSM) and central composite design (CCD) to predict overall material performance. A comprehensive investigation was conducted to understand how various processing parameters influence the mechanical and adhesive performance of the composite materials. Optimized process parameters were proposed to ensure the composite material achieved optimal performance. Additionally, mechanical verification was carried out for the optimized parameters. Scanning electron microscopy (SEM), confocal laser scanning microscopy (CLSM), and Fourier transform infrared spectroscopy (FTIR) were utilized to investigate the adhesive mechanism of the scored bamboo laminations.

## 2. Materials and Methods

### 2.1. Materials

Moso bamboo (*Phyllostachys edulis*) (4 years old) was obtained from Jinzhai County, Anhui Province, China. Poplar veneers with a nominal thickness of 3 mm were sourced from the Poplar Board Production Base in Heze City, Shandong Province. The average moisture content of the veneers was around 12%, and the average air-dry density was 0.37 g/cm$^3$. Phenolic resin (PF) was obtained from Jinzhai CIMC New Materials Technology Development Co., Ltd., Lu'an, China, with a viscosity of 2500 mPas, solid content exceeding 47%, and a pH value of 11.

### 2.2. Preparation of Bamboo–Wood Composites

#### 2.2.1. Preparation of Grooved-Flattened Bamboo (GFB) Units

Figure 1a illustrates the manufacturing process of the GFB units. The fresh bamboo culms were cut into 3–4 strips with a thickness of 8 mm and then fed into a specific device for the integrated preparation of GFB units. In this equipment, bamboo units underwent three treatments, namely, flattening, removing the bamboo culm outer and inner layers, and grooving. Firstly, pressure rollers flattened the arc-shaped bamboo strips, and carving knives on these rollers were responsible for creating slots on the bamboo surface. This method was direct and rapid, allowing the flattening of bamboo strips with a large width (up to approximately 10 cm). Additionally, the internal stress of bamboo generated during the flattening process was released through slotting, which contributed

to improved dimensional stability. Secondly, the inner layer and outer layer of the flattened bamboo strips were removed, exposing the porous structure, and thereby guaranteeing the material's bonding stability. Thirdly, the bamboo strips underwent grooving treatment to achieve surfaces with a consistent "V" configuration, enhancing the robustness of the gluing area. Finally, GFB units with a final thickness of 5.5–7.5 mm were obtained and then conditioned to achieve a moisture content of 8%–10%.
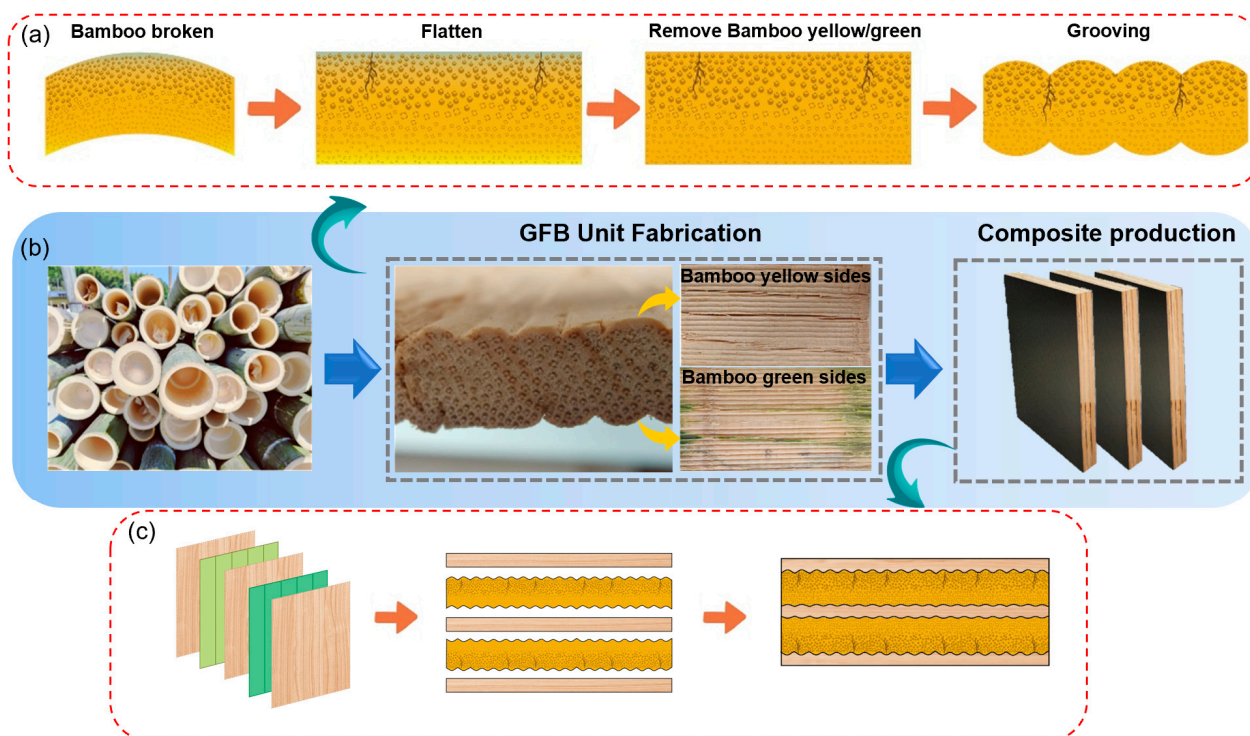


**Figure 1.** Preparation of bamboo–wood composite laminated boards: (**a**) GFB fabrication, (**b**) preparation of bamboo–wood composite, and (**c**) bamboo–wood composite structure.

### 2.2.2. Structural Design of Bamboo–Wood Composites

The prepared GFB and wood veneer were sawn into boards measuring 750 mm (length) × 34 mm (width) × 6.8–7 mm (thickness) and 750 mm (length) × 34 mm (width) × 1.5 mm (thickness), respectively. The layup structure of the bamboo–wood composite is shown in Figure 1c. To mitigate the stress concentration defects introduced by grooving in GFB, this study designed a five-layer composite structure in which three wood layers were alternated with two GFB layers, and their grain directions were perpendicular. The grooves on the GFB surface increased the contact area, and the softness of the wood layers facilitated a good fit with the wavy adhesive interface. Finally, PF-impregnated film papers covered the surfaces of the composites.

It is noteworthy that to facilitate a performance comparison, the as-received bamboo culms were divided into three sections. After undergoing high-temperature steam softening at 180 °C for 70 min, the bamboo slices were subsequently treated to remove the green and yellow layers. Then, these sections were flattened through rollers, resulting in homogeneous flat bamboo units. Finally, flat bamboo–wood composites were crafted, adhering to a consistent five-layer structural design.

### 2.3. Optimization of Process Parameters for Bamboo–Wood Composite Production

In this study, we employed the central composite rotatable design (CCRD), a widely recognized approach in response surface methodology (RSM), to optimize the hot-pressing parameters for bamboo–wood composite production. The CCRD methodology, acknowledged for its effectiveness in process modeling, analysis, and optimization, facilitates the

efficient exploration of parameter effects while accommodating both linear and quadratic effects, along with interactions, within a minimal number of experiments [11,12]. To prepare bamboo–wood composites with a stable structure and controllable properties, we conducted a systematic study on three key hot-pressing parameters. The three parameters under scrutiny encompass the hot-pressing time, pressure, and hot-pressing temperature. To explore the relationship between these parameters and material performance more meticulously and accurately, we set three different levels for each parameter. Drawing from a wealth of experimental findings and literature references [13], Table 1 encapsulates the process parameter values and their corresponding tiers as addressed in this research.

**Table 1.** Experimental design scheme of the response surface.

| Level | A (Temperature, °C) | B (Hot-Pressing Time, min/mm) | C (Pressure, MPa) |
|---|---|---|---|
| −1 | 110 | 1 | 1 |
| 0 | 130 | 1.2 | 1.5 |
| 1 | 150 | 1.4 | 2 |

The modulus of rupture (MOR) and modulus of elasticity (MOE) of the bamboo–wood composites, prepared under different process parameter conditions, were measured by a universal mechanical testing machine (5528, Instron Corporation, Norwood, MA, USA) according to GB/T17657-2013 [14]. They were taken as the measured response values. The relationship between the influencing factors and response values was established using Design-Expert software (v8.0.6, Stat-Ease, Inc., Minneapolis, MN, USA). During the model-building process, random experiments were conducted to avoid the introduction of systematic errors into the system. With the assistance of the Design-Expert software and operating at a 95% confidence interval, we deduced coefficients pertinent to the second-order polynomial regression model. Furthermore, to ensure the accuracy of the developed model, an analysis of variance (ANOVA) was performed, including significance tests for the regression model and its coefficients.

*2.4. The Tensile Shear Properties of Bamboo–Wood Composites*

The tensile shear test, employed to ascertain the adhesive strength of materials, adheres to the national standard GB/T17657-2013 [14]. Samples were meticulously crafted from the board, each measuring 100 mm in length and 25 mm in width. For each board, three specimens were prepared to evaluate the dry-bonding strength of the material. Utilizing a 100 kN sensor, an optimal load speed was chosen to ensure the specimens reached failure within a precise window of 60 ± 30 s. Upon the specimens' failure, a detailed examination of the fracture surfaces was conducted to gather insights into the bonding efficacy.

To compare the mechanical response between the grooved bamboo composite and homogenous bamboo composite, finite element analysis was employed. The tension specimens were modeled using Autodesk CAD v2023 software (Autodesk, San Francisco, CA, USA), and the strain distribution in the material during tension was studied using ANSYS v12.1 software (ANSYS Inc., Canonsburg, PA, USA). The MOR and MOE of the GFB were 45.96 MPa and 1557.95 MPa, respectively [10]. The average bending modulus of the wood veneer was 10,615 MPa, the tensile modulus was 11,339 MPa, and the maximum tensile stress was 28.42 MPa [15]. Cohesive elements were incorporated at the interface between the wood and bamboo layers to analyze the effectiveness of the adhesive bonding. The transverse shear behavior of the cohesive units was quantified by the changes in the position of the upper and lower surfaces perpendicular to the direction of thickness. Notably, the cohesive units employed a bilinear constitutive model. Thus, the damage process at the adhesive interface mainly encompassed two stages: initiation of damage and propagation. The damage propagation followed the Bishop–Kuwabara Failure Criterion [16]. The tensile process of the material was achieved by fixing the left end and applying tensile displacement at the right end.

### 2.5. Bonding Interface and Mechanism

The physical bonding mechanisms between bamboo and wood in composite materials were investigated using a scanning electron microscope (SEM) (GeminiSEM360, Zeiss, Oberkochen, Germany) and confocal laser scanning microscopy (CLSM) (LSM510Meta, Zeiss, Oberkochen, Germany). SEM was used to observe the microstructural characterization of the GFB unit and the bonding surface of the bamboo–wood composite. The acceleration voltage was 5 kV. CLSM was used to observe the glue distribution at the adhesive interface. The bamboo–wood composites were cut into 20 μm thick cross-sections using a sliding microtome, stained for 1 h with 0.5% toluidine blue, washed with deionized water, and sealed with a mixture of glycerol and water at a 1:1 ratio. The prepared slides were observed using CLSM, with the laser wavelength set at 488 nm and the laser current set at 6.5 A.

The chemical bonding mechanisms between the resin and bamboo unit were studied using Fourier transform infrared (FTIR) spectroscopy (Thermo Fisher, Perkin Elmer, Inc., Shelton, CT, USA). The FTIR spectra samples were obtained from 20 μm thick cross-sectional slices prepared by slicing. Specifically, samples were carefully selected from targeted areas within the bamboo–wood composites, such as the bamboo unit areas and areas close to the adhesive layers, to ensure the representativeness and relevance of the results. The FTIR spectra were recorded with a spectral resolution of 4 $cm^{-1}$ in the range of 4000 $cm^{-1}$ to 400 $cm^{-1}$.

### 2.6. Penetration of Water

Contact angles were used to assess the surface hydrophilicity of the pith ring side of natural bamboo, the inner side of flat bamboo without the pith ring, and the inner side of GFB. The dynamic changes in the contact angles of the water droplets on the bamboo's green side were measured with contact angle apparatus (OCA20, Dataphysics Ltd., Filderstadt, Germany) utilizing an automatic circle-fitting approach, and the droplet volume was set at 3 μL. For consistency of the experimental outcomes, the experiment was conducted three times. Once the water droplet formed and left the syringe needle, the image was captured for 20 s and recorded by a CCD camera.

## 3. Results

### 3.1. Numerical Modeling and Effectiveness Assessment

The optimal response of an empirical model was established through response surface methodology, as shown in Table 2. Employing the Design-Expert statistical software, the F test was used to ascertain the significance of all the coefficients at a 95% confidence interval. The mathematical relationship between each factor and developmental response was explained using the 2FI model [17]. After determining the significant coefficients, a mathematical model to estimate the MOR (1) and MOE (2) of the composite material based on coded factors can be obtained, as shown below:

$$MOR = 112.54 + 9.49A - 0.3994B - 0.2489C + 0.0475AB - 0.0525AC \\ +0.165BC - 0.4299A^2 - 1.97B^2 - 1.49C^2 \tag{1}$$

$$MOE \ (Gpa) = 10.89 + 0.6627A - 0.1269B - 0.0707C + 0.085AB + 0.0875AC \\ +0.0775BC - 0.2003A^2 - 0.1243B^2 - 0.3064C^2 \tag{2}$$

The appropriateness of the developed model was then evaluated using ANOVA. The statistical results of the ANOVA are presented in Table 3. At the 95% confidence level, the calculated F-ratio is greater than the tabulated value, which proves that the model is adequate. The coefficient of determination ($R^2$) is also widely used to assess the reliability of fitted regression models. A higher $R^2$ value (with a maximum of 1) and a lower standard error (SE) indicate that the regression model is very reliable and can be used to predict the response. In the context of these crafted models, both the computed and adjusted $R^2$ values surpass 90% and 80%, respectively, indicating the high reliability of the regression model.

Additionally, the coefficient of variation (CV) indicates the degree of deviation of the unit output from the mean. The CV values in Table 3 are low, indicating the precision and reliability of the conducted experiments. A value of "Prob > F" less than 0.0500 indicates that the model also possesses statistical significance.

**Table 2.** Experimental design matrix and corresponding responses.

| Std Order | Run Order | Point (a) | Input Parameters | | | Output Parameters | |
|---|---|---|---|---|---|---|---|
| | | | A | B | C | MOR, MPa | MOE, GPa |
| 1 | 7 | F1 | 110 | 1 | 1 | 100.12 | 10.16 |
| 2 | 8 | F1 | 150 | 1 | 1 | 121.54 | 11.12 |
| 3 | 2 | F1 | 110 | 1.4 | 1 | 99.89 | 9.55 |
| 4 | 12 | F1 | 150 | 1.4 | 1 | 120.46 | 11.1 |
| 5 | 1 | F1 | 110 | 1 | 2 | 98.72 | 9.43 |
| 6 | 16 | F1 | 150 | 1 | 2 | 118.89 | 10.99 |
| 7 | 13 | F1 | 110 | 1.4 | 2 | 98.11 | 9.38 |
| 8 | 14 | F1 | 150 | 1.4 | 2 | 119.51 | 11.03 |
| 9 | 9 | A1 | 96.3641 | 1.2 | 1.5 | 96.21 | 9.22 |
| 10 | 11 | A1 | 163.636 | 1.2 | 1.5 | 123.56 | 11.2 |
| 11 | 4 | A1 | 130 | 0.863641 | 1.5 | 106.75 | 10.75 |
| 12 | 6 | A1 | 130 | 1.53636 | 1.5 | 104.28 | 10.1 |
| 13 | 3 | A1 | 130 | 1.2 | 0.659104 | 105.88 | 9.87 |
| 14 | 17 | A1 | 130 | 1.2 | 2.3409 | 107.89 | 9.95 |
| 15 | 10 | C1 | 130 | 1.2 | 1.5 | 113.1 | 10.89 |
| 16 | 15 | C1 | 130 | 1.2 | 1.5 | 112.44 | 10.91 |
| 17 | 5 | C1 | 130 | 1.2 | 1.5 | 112.56 | 10.92 |

(a) F1 factorial point, A1 axial point, C1 center point.

**Table 3.** ANOVA table for the response surface model.

| Terms | Responses | |
|---|---|---|
| | MOR, MPa | MOE, Gpa |
| Sum of squares | | |
| Regression | 1288.17 | 7.66 |
| Residual | 47.2 | 0.3503 |
| Lack of fit | 46.95 | 0.3498 |
| Pure error | 0.2472 | 0.0005 |
| Mean squares | | |
| Regression | 143.13 | 0.8511 |
| Residual | 6.74 | 0.05 |
| Lack of fit | 9.39 | 0.07 |
| Pure error | 0.1236 | 0.0002 |
| Degrees of freedom | | |
| Regression | 9 | 9 |
| Residual | 7 | 7 |
| Lack of fit | 5 | 5 |
| Pure error | 2 | 2 |
| Std. Dev | 2.6 | 0.2237 |
| Mean | 109.41 | 10.39 |
| C.V.% | 2.37 | 2.15 |
| PRESS | 357.17 | 2.7 |
| $R^2$ | 0.9647 | 0.9563 |
| Adj $R^2$ | 0.9192 | 0.9 |
| Adeq Precision | 16.0218 | 12.9913 |
| F-ratio (calculated) | 21.23 | 17.01 |
| Prob F | 0.0003 | 0.0006 |
| Remark | Significant | Significant |

*3.2. Effects of Process Parameters on Responses*

The duration of hot pressing, applied pressure, and hot-pressing temperature are key process parameters in the production of bamboo–wood composites [18]. They directly affect the effectiveness of bonding curing and thereby the properties of the composite material. In general, these three processing parameters interact to collectively define the overall properties of bamboo–wood composite materials. To obtain the best performance, these parameters need to be meticulously fine-tuned and optimized during experiments. In the following sections, the other parameters are thought to be at their center levels whenever an interaction effect or a comparison between any two input parameters is being discussed.

### 3.2.1. The Response of MOR

Figure 2 illustrates the 2D contour interactions among any two treatment parameters affecting the MOR. A notable positive correlation was observed between the MOR and the temperature during hot pressing (Figure 2a,b). It can be inferred that higher hot-pressing temperatures enhance the flowability and penetrability of the adhesive and effectively improve the physical bonding and chemical bonding ability between PFs and bamboo–wood composites. Conversely, the effects of hot-pressing time and pressure on the MOR are less significant. Intriguingly, as the hot-pressing time and pressure increase, the MOR first increases and then tends to decrease. This is presumed to be due to the inadequate dispersion of the adhesive under shorter durations and lower pressures of hot pressing, resulting in weaker bonding. On the other hand, grooving treatment leaves numerous stress concentration areas on the bamboo surface, and higher pressure and prolonged hot pressing may reduce the stability of GFB, leading to localized crack initiation. Therefore, to achieve optimal bending strength, it is necessary to consider the appropriate pressure and hot-pressing time to ensure the uniform distribution of the adhesive and the densification of the material.
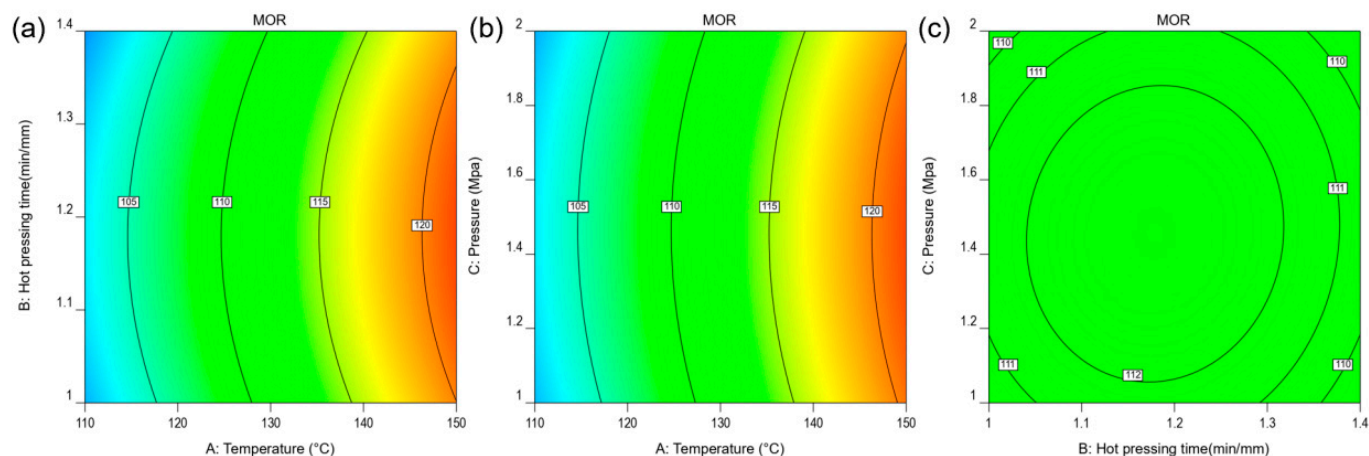


**Figure 2.** Response of the MOR to the process parameters: (**a**) hot-pressing temperature and time; (**b**) hot-pressing temperature and pressure; (**c**) hot-pressing time and pressure.

### 3.2.2. The Response of the MOE

Figure 3 clearly shows the effects of the different processing parameter combinations on the MOE of the bamboo–wood composite materials. As observed, the range of MOE variation is primarily between 9 and 11 GPa. The influence mechanism of the processing parameters on the MOE is similar to that on the MOR. Specifically, higher temperatures during hot pressing aid in enhancing the MOE of bamboo–wood composites (Figure 3a,b). An increase in hot-pressing time and pressure similarly promoted an initial increase followed by a decrease in the MOE. Distinctly, within the experimental parameter range of this study, the effect of pressure on the MOE is more pronounced than that of hot-pressing time, as depicted in Figure 3c. This greater variability, introduced by pressure, is due to

the instability of the GFB caused by the scoring treatment. Hence, to optimize the MOE of bamboo–wood composite materials, careful selection of the appropriate pressure is necessary to ensure consistency during the hot-pressing process.
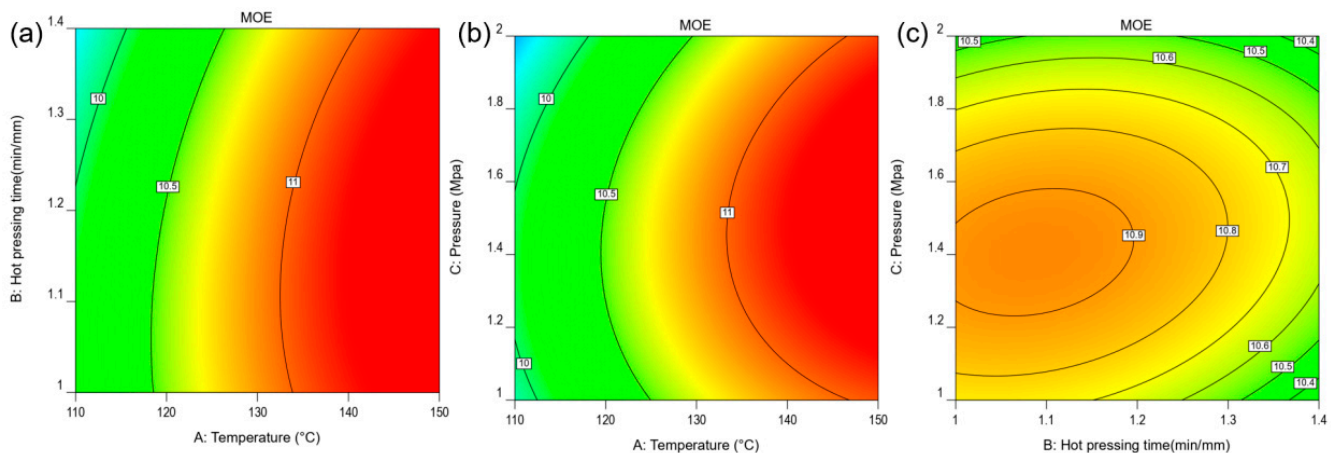


**Figure 3.** Response of the MOE to the process parameters: (**a**) hot-pressing temperature and time; (**b**) hot-pressing temperature and pressure; (**c**) hot-pressing time and pressure.

### 3.2.3. Optimization and Verification of the Effects of the Process Parameters on the Responses

The findings from the previous section reveal that the process parameters exhibit a more complex response to the material's mechanical properties. Therefore, it is imperative to select the appropriate process parameters to endow bamboo–wood composites with the desired performance combination. As mentioned above, the primary advantage of the RSM is optimizing the response by manipulating the independent variables [13]. Optimization aims to determine the best mechanical performance within the experimental realm of processing parameters [19]. For the sake of optimization, numerical and graphical methods were employed by selecting the favored goals for the parameters and responses, as demonstrated in Table 4.

**Table 4.** Goals and limitations considered in the optimization process.

| Name | Goal | Lower Limit | Upper Limit |
|---|---|---|---|
| A: Temperature | In range | 110 | 150 |
| B: Hot-pressing time | In range | 1 | 1.4 |
| C: Pressure | In range | 1 | 2 |
| MOR | Maximize | 96.21 | 123.56 |
| MOE | Maximize | 9.22 | 11.2 |

A desirability-based approach was employed to evaluate the optimization results. The desirability of each factor, which ideally ought to closely approach 1, contributes to comprehensive optimization [20]. The computed findings revealed an optimized comprehensive desirability of 0.962 in this research, signifying congruence between the optimized input and target output values (Figure 4a). It has been established in earlier discussions that the temperature during hot pressing is positively correlated with the overall mechanical performance of the material. Consequently, Figure 4b,c depicts the response surface and corresponding contour map of the interaction effects between hot-pressing time and pressure on the response surface at 150 °C, which illustrates a graphical search for potential optimal cooperation. The higher composite desirability further confirms the consistency between the mechanical properties and bonding strength. Specifically, the quantified results also suggest that the optimal lamination conditions for bamboo–wood composites are a hot-pressing duration of 1.18 min/mm, 1.47 MPa of pressure, and a hot-pressing

temperature of 150 °C. Under these parameters, the optimal values for the MOE and MOR of the bamboo–wood composite material are 121.625 MPa and 11.354 GPa, respectively.
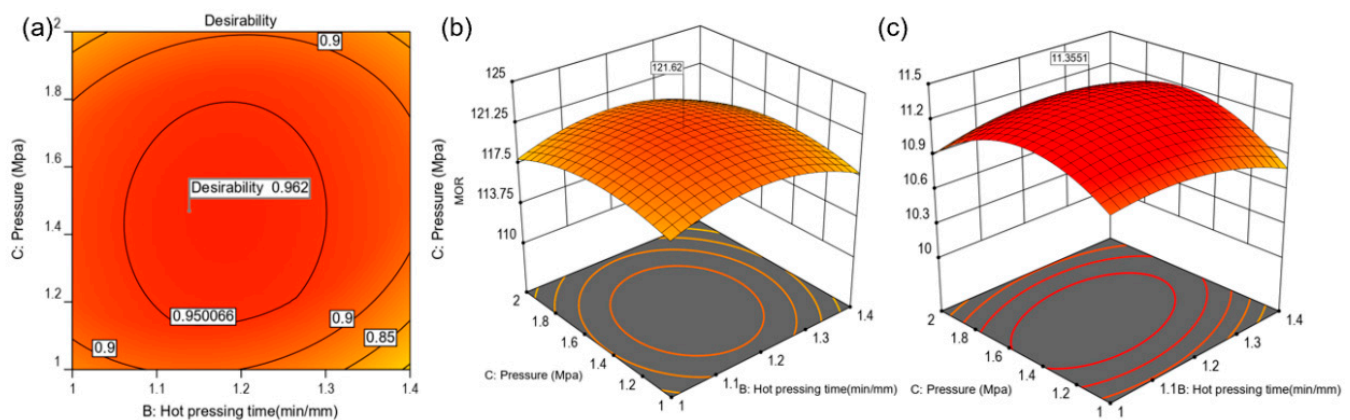


**Figure 4.** Response surface and corresponding contour plots of 2D optimization diagrams determined by desirability (**a**) and the interaction between hot-pressing time and pressure at 150 °C (**b**,**c**).

Subsequent verification experiments were further conducted, as shown in Figure 5a. The mechanical properties of the grooved bamboo composites prepared under the optimized conditions were tested three times, and exhibited an error of only ~5% for the mechanical properties predicted by RSM, with an average MOR and MOE of 121.51 MPa and 11.85 GPa, respectively. To further verify the adhesive capability of the material, we compared the three-point bending and mechanical responses of the grooved bamboo and homogeneous flat bamboo composite materials. The grooved bamboo composite material displayed a mechanical response similar to that of the flat bamboo composite. If the highest point of the stress–strain curve in Figure 5a is regarded as the start of crack initiation, the curve can be divided into two stages: the elastic–plastic stage (the E&P stage) and the crack propagation stage (the C-stage). During the elastic–plastic stage, both the grooved and flat bamboo composite materials exhibited almost identical performances, indicating that the grooving treatment had little effect on the MOE of the composite material. This might be because the elastic deformation of the side-bonded bamboo integrated material is related only to the performance of the unit, and the bonding performance between the units has little impact on it. However, the grooving treatment had some effect on the MOR of the material. The MOR of the grooved bamboo composite material was slightly less than that of the flat bamboo composite. This decrease could be due to the preset cracks causing the initiation of cracks. For the C-stage, the crack propagation stage exhibits noticeable fluctuations. This is primarily because, unlike single materials, the structural characteristics of laminated composite materials determine their ability to suppress the generation of local stress during the plastic deformation process and delay the phenomenon of strain localization. Interestingly, the C-stage of the grooved bamboo laminate is significantly longer, which is related to the unique milling structure of the device, which will be further discussed later in the text. Furthermore, we calculated the areas enclosed by the curves of the different stages and assessed the energy absorption capacity of the material in each stage based on the formula [21]

$$W = \int_0^d F dx$$

where F is the applied force and d is the total displacement at different stages. The specific calculation results can be seen in Figure 5b. Through this quantitative evaluation method, we found that homogeneous flat bamboo composites demonstrated superior performance during the elastic–plastic deformation stage. However, during the crack propagation stage, the energy absorption capacity of the grooved bamboo composites reached twice that of the composite structure without grooving.
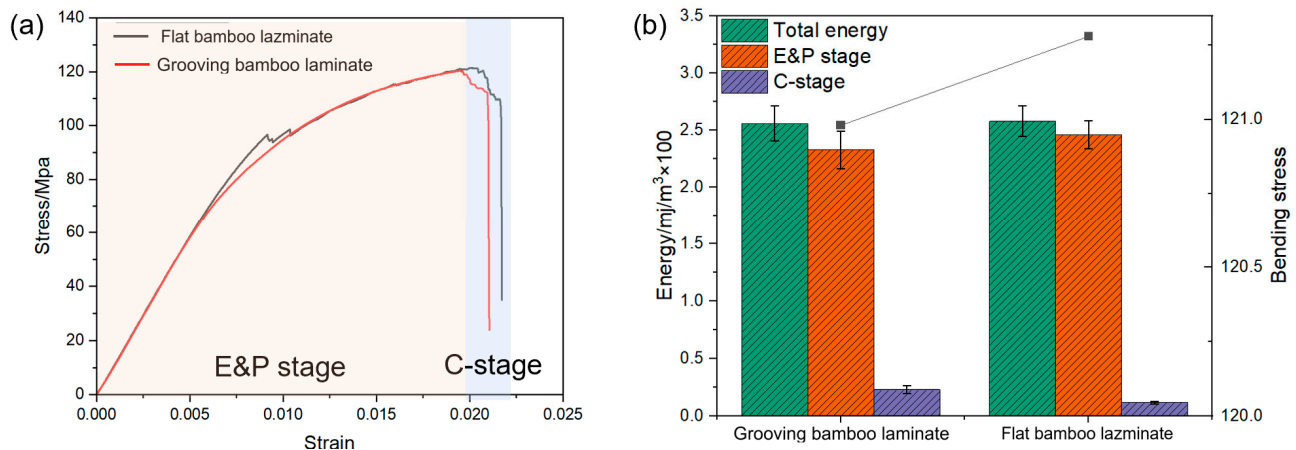
**Figure 5.** Three-point bending mechanical responses of bamboo–wood composites based on grooved bamboo and flat bamboo: (**a**) stress—strain curve; (**b**) energy absorption capacity at different stages of the tensile process.

### 3.3. The Tensile Shear Properties of Bamboo–Wood Composites

Enhancing our understanding of the ductile behavior of cracks in grooved bamboo composite materials necessitated conducting experiments on samples with pre-introduced grooves with a 3 mm width, subjected to double-ended stretching. The structures of these experiments are depicted in Figure 6. As observed, cracks predominantly originate within the bamboo–wood adhesive layer. Observations indicate that the propagation of cracks is significantly influenced by the softer layer's structure, attributable to the lower strength of the wood side. This influence steers the crack paths, causing deviations that culminate in the emergence of three distinct fracture morphologies: interlayer, fracture, and shear cracks.
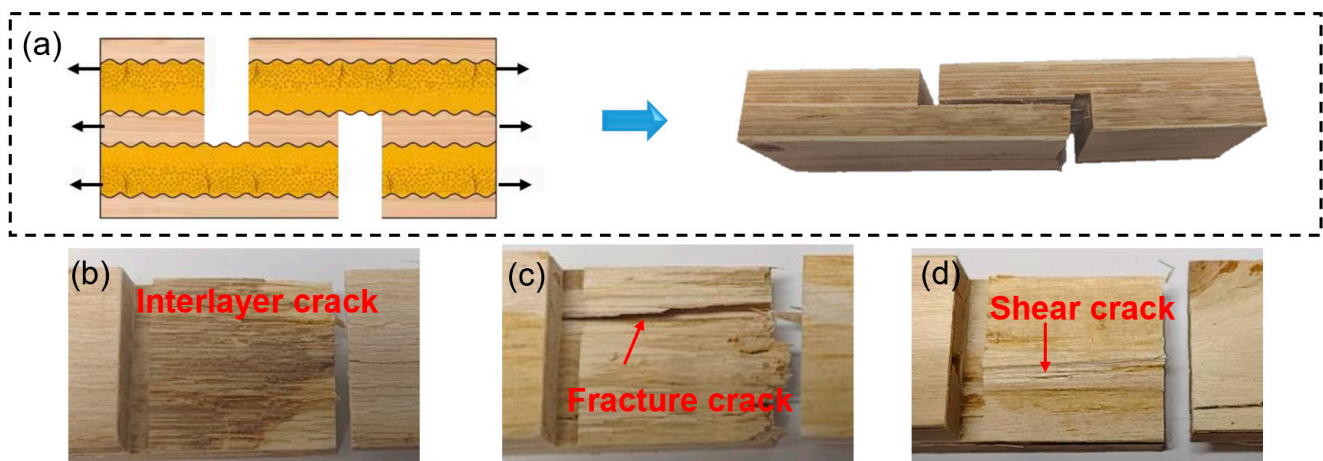


**Figure 6.** Tensile shear responses of bamboo–wood composites: (**a**) tensile diagram and fracture morphology; (**b**–**d**) typical fracture mechanism.

We further conducted tensile simulation tests on bamboo–wood composite materials using ANSYS to further explore the mechanical response of the material. As depicted in Figure 7, the evolutions of the stress distribution during the tensile process in both homogeneous flat bamboo and grooved bamboo composites can be observed. As observed, different structures under tensile action exhibited similar macroscopic stress distributions, which essentially corresponded to the maximum shear force direction at 45°. However, the locations of stress concentration between the two are noticeably different. For the flat bamboo composite material, the stress is more uniformly distributed around the notches, while for the grooved bamboo composite material, the stress is more concentrated at

the wavy milling grooves in the notches, where there is a smaller cross-sectional area. This phenomenon reveals that preset grooves would introduce a degree of stress concentration. Interestingly, the grooved bamboo composite material could withstand larger displacements. At a displacement of 0.14 mm, the adhesive junction of the flat bamboo composite exhibited significant stress concentration and crack propagation. In contrast, for the grooved bamboo composite material, delamination was observed only when the displacement reached 0.19 mm, where the stress peaked at 95.96 MPa. It can be inferred that grooved bamboo, to a certain extent, possesses greater elasticity and load-bearing capacity, enabling it to remain intact under greater displacements without breaking easily. These characteristics are directly related to the smaller bearing area and preset engraving cracks in the grooved bamboo. To substantiate this hypothesis, as shown in Figure 7d, we further studied the stress evolution during the delamination process. The stress transmission in the flat bamboo structure is more continuous. The homogeneous structural features of the flat bamboo suggest that the crack propagation encounters less resistance. However, the stress transmission in the grooved structure clearly exhibits discontinuity. During the crack propagation process, the stress transmission undergoes additional orientation rotations. On the other hand, the irregular wavy features in the grooved structure introduce an alternating change between the soft and hard layers, leading to increased resistance during crack propagation. Therefore, it can be inferred that the wavy bamboo morphology formed by milling increases the bonding area of bamboo, which can effectively increase the energy absorption and comprehensive mechanical properties at the fracture stage.
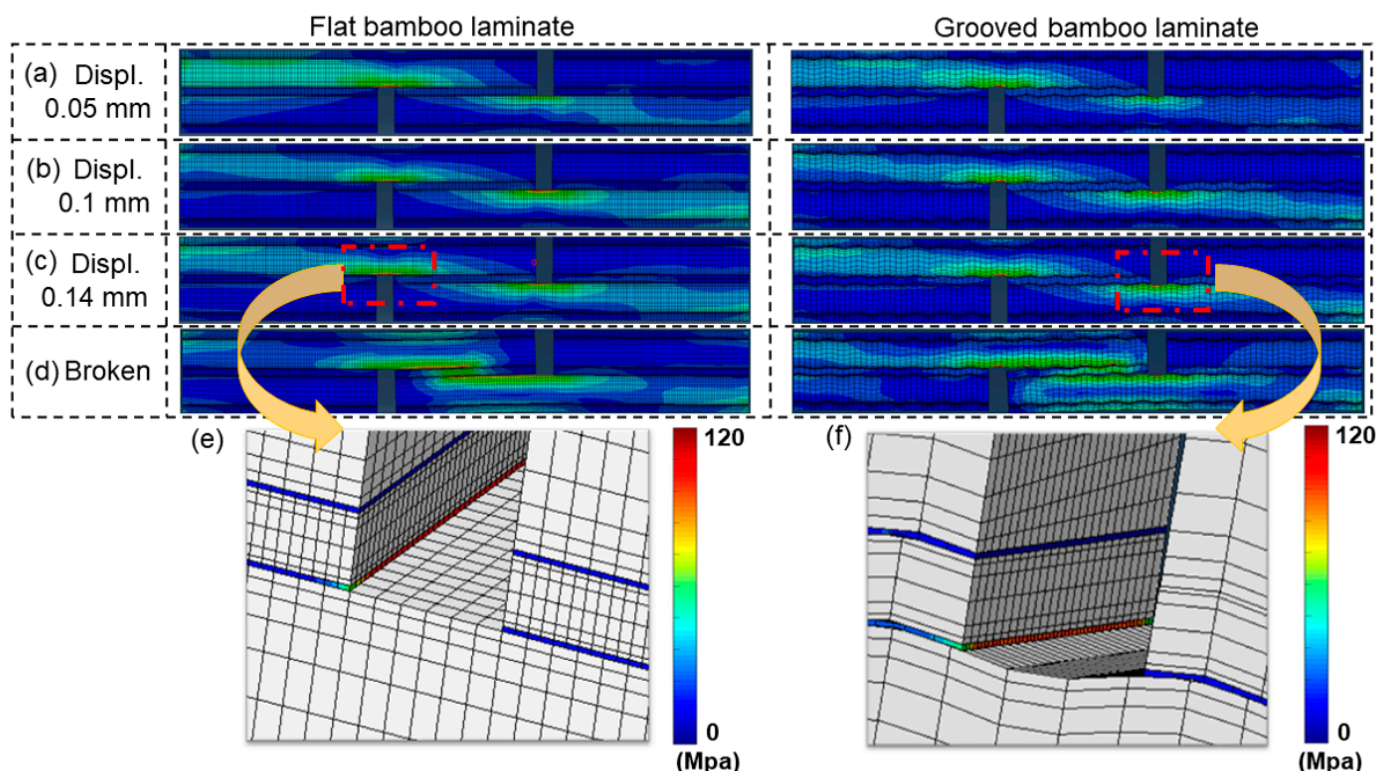


**Figure 7.** Strain distribution of grooved bamboo laminates and flat bamboo laminates in tension using FEM: (**a**–**d**) the stress distribution at different displacements until failure; (**e**,**f**) the stress distribution in the adhesive layer at a displacement of 0.14.

### 3.4. Bonding Mechanism

The most crucial aspect of bamboo–wood composite material performance lies in the bonding capacity between its various layers. Figure 8a–c shows the SEM images of the GFB surface, where Figure 8a shows the inner part of bamboo and Figure 8c shows the outer part of bamboo. The grooving treatment led to the disappearance of the cortex and pith

ring and the exposure of fine pores. Larger grooving depths essentially expose a greater proportion of the parenchymal cells of bamboo, while also reducing the anisotropy between the outer and inner sides of the bamboo. This process plays a positive role in enhancing the stability of bamboo–wood composite materials. To determine the impact of grooving treatment on the material permeability, we further compared the wettability of the pith ring side of natural bamboo (NB), the inner side of flat bamboo without the pith ring (FB), and the inner side of GFB (Figure 8f). The initial contact angle of the bamboo pith ring after sanding decreased from 95° to 73°. However, compared to that on the flat bamboo which had the pith ring sanded, the change on the GFB surface was not significant and only decreased by 2°, indicating that both processes effectively disrupted the smooth surface of the bamboo. Nonetheless, there was a marked difference in the final wettability of the three materials, with contact angles of 79.87°, 65.13°, and 27.66°. The liquid on the surface of the GFB almost entirely permeated into the bamboo, demonstrating that grooving could improve the permeability of the bamboo more effectively.
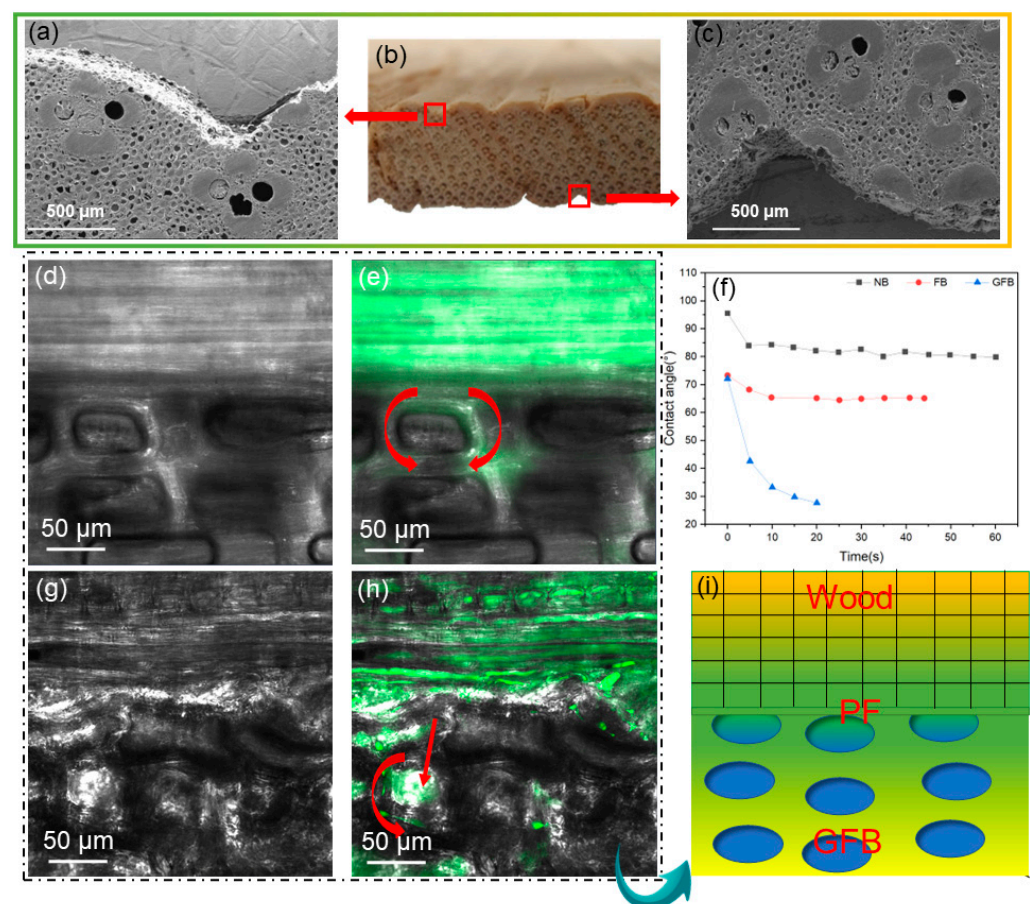


**Figure 8.** Mechanism of physical bonding. (**a**–**c**) SEM image of the grooved bamboo's inner side and the bamboo's outer side. (**d**,**e**) CLSM images of the composite interface of non-grooved bamboo before and after gluing. (**f**) The contact angles of the NB, FB, and GFB. (**g**,**h**) CLSM images of the composite interface of grooved bamboo before and after gluing. (**i**) The physical bonding mechanism of gluing.

Figure 8d,g displays the composite interface of the grooved bamboo and non-grooved bamboo. The parenchymal cells in the non-grooved bamboo still maintained their complete cell wall structure during the hot-pressing process. After bonding, CLSM revealed that the substance penetrating the cavities and cell walls of parenchymal cells was PF (Figure 8e). Compared to those of fiber cells, the cell walls of parenchymal cells are thinner, the cell cavities are larger, and the cell walls have dense pits, which are more conducive to the

penetration of glue [22]. Furthermore, the damaged parenchymal cells of grooved bamboo at the bonding interface exhibited significant fracturing due to hot pressing. The cavities of cells at the adhesive interface were filled with a substance identified as PF based on CLSM (Figure 8h). It can be inferred that PF can penetrate cell walls via the pits present on the cells. Overall, PF could penetrate parenchymal and fiber cells more effectively after grooving, forming a more stable glue–nail network structure (Figure 8i).

Chemical bonding is an essential reason for the formation of gluing forces [23]. Figure 9 illustrates the infrared spectral differences between grooved bamboo composites and homogeneous flat bamboo composites, revealing the chemical reaction mechanism of PF with the cells of bamboo. In the respective infrared spectra, the peak at 1738 cm$^{-1}$ is attributed to the stretching vibration of the C=O ester carbonyl (hemicellulose) in bamboo. The peak at 1601 cm$^{-1}$ is likely the result of the stretching vibration of the aromatic ring in PF and the bending vibration of C-H. Moreover, the chemical reaction between PF and bamboo results in a more complex infrared spectral response, which significantly fluctuates in the 1300–1500 cm$^{-1}$ intensity range, where the peak at 1516 cm$^{-1}$ is likely due to benzene ring stretching. The peak at 1460 cm$^{-1}$ is attributed to the asymmetric stretching vibration of C-H/symmetric deformation vibration of CH. The peak at 1426 cm$^{-1}$ is attributed to the scissoring vibration of CH2. The peak at 1368 cm$^{-1}$ is attributed to the bending of aliphatic CH in cellulose and hemicellulose. The most prominent peaks at 1242 cm$^{-1}$, 1159 cm$^{-1}$, and 1032 cm$^{-1}$ are associated with the stretching vibrations of C-O in cellulose and hemicellulose. Compared with the flat bamboo laminates, grooved bamboo laminates show a similar intensity of the above peaks. It can be indicated that the grooving treatment will not cause deterioration of the chemical reaction at the interface.
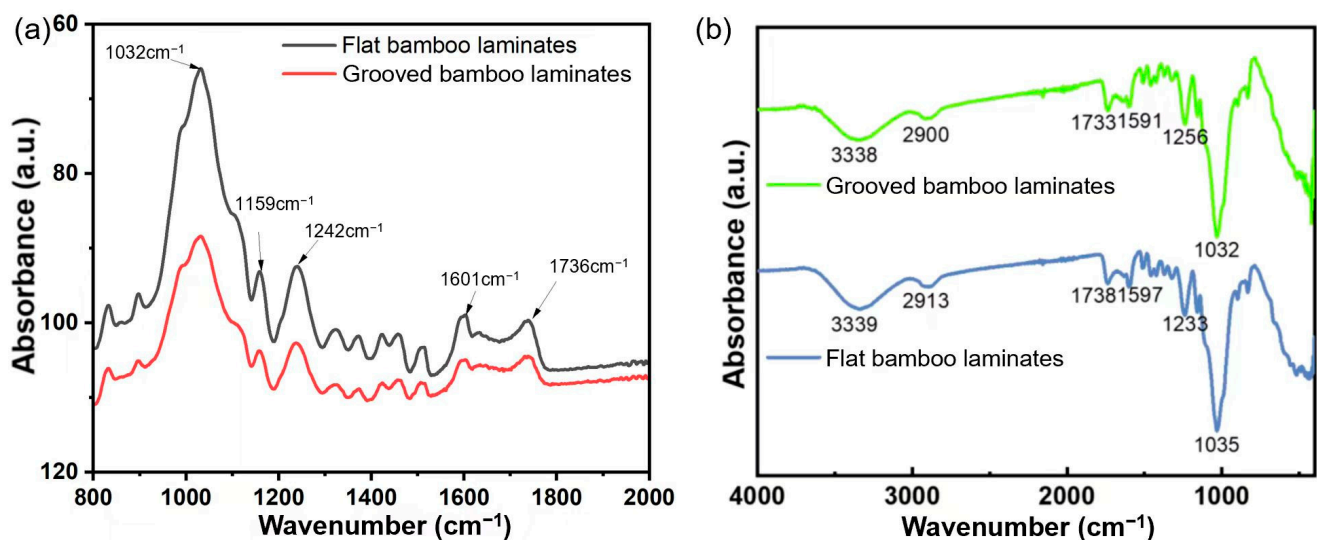


**Figure 9.** (**a**) Infrared spectra and (**b**) infrared difference spectrum of grooved bamboo laminates and flat bamboo laminates near the adhesive layer.

## 4. Application

The bonding area is an important factor affecting adhesion. Research shows that increasing the bonding area can effectively improve bonding stability [17,24]. In the present study, we also found that milling can effectively increase the energy absorption and mechanical properties of bamboo at the fracture stage by increasing the gluing area of bamboo. Hence, by manipulating the cutting blades and modifying the number and shape of the arc-shaped protrusions, we were able to adjust the ratio of the bonding area, thus improving the designability of the system. As shown in Figure 10a–c, the wavy surface milling pattern resembles a cycloid. Therefore, by controlling the blades of the milling cutter, the shape and number of arc-shaped protrusions are altered, thereby increasing the proportion of the gluing area. In this study, to simplify the calculations, an approximate

circular method is employed to analyze the area changes introduced by scoring. The increased gluing area ratio due to the surface milling pattern can be estimated using the following formula:

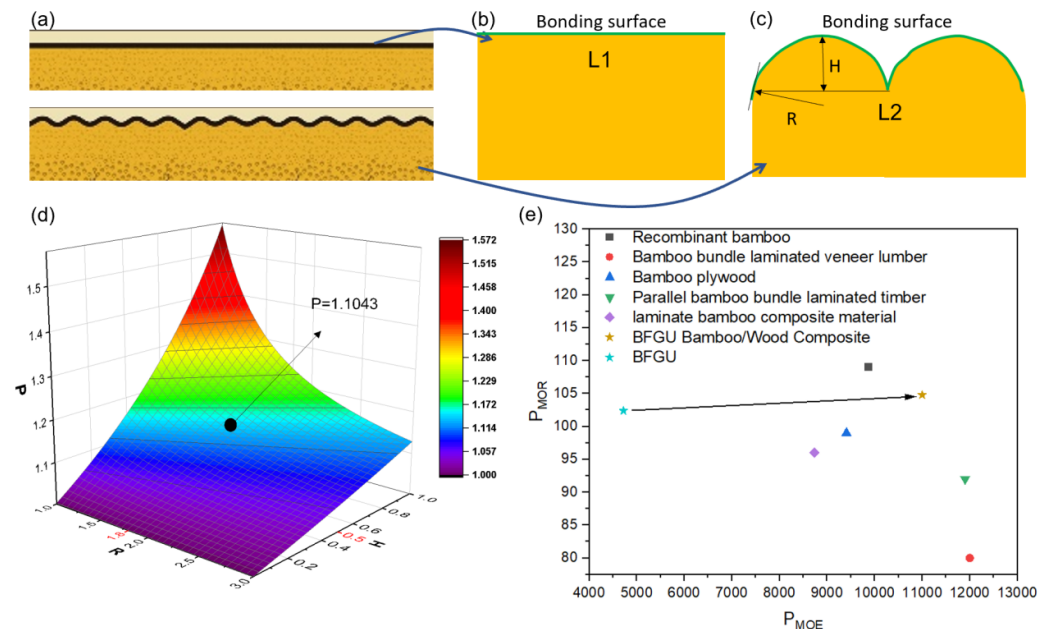$$P = \frac{L_2}{L_1} = \frac{\arccos(1 - \Delta)}{\sqrt{1 - \left(1 - \Delta\right)^2}}$$



**Figure 10.** (**a**–**c**) Increased gluing area ratio due to surface milling pattern. (**d**) Impact of arc-shaped milling pattern on gluing area ratio. (**e**) Comparison of comprehensive properties of different bamboo materials.

Here, $\Delta$ represents the ratio of the height H of the arc-shaped milling pattern to the radius R of the circular arc-shaped milling pattern. Figure 10d shows the impact of the height H and the radius R of the arc-shaped milling pattern on the gluing area ratio. As observed, the milling height H is negatively correlated with the gluing area ratio, while the other factors are the opposite. Considering the decrease in bamboo volume due to scoring, a moderate score was chosen for this study, with R being 1.8 mm and H 0.5 mm. The corresponding gluing area ratio is 1.1043, indicating that the area of the wavy milling pattern is ~10% greater than that of ordinary flattened bamboo. To integrate the mechanical properties and adhesive stability and to provide a comprehensive mechanical assessment of the bamboo–wood composite materials, an area-weighted performance index was introduced:

$$P_{MOE} = MOE \times P$$

$$P_{MOR} = MOR \times P$$

Based on the above equation, we compared the modification properties of several different bamboos [7,25–30], as shown in Figure 10e. It is evident that bamboo–wood composites utilizing GFB units demonstrate excellent comprehensive performance. Specifically, compared to that of GFB units, the composite performance of bamboo–wood materials was significantly improved. After the flattened bamboo sheets and wood veneers were combined, the surface defects were filled, and due to the increased bonding area, the mechanical properties of the final laminated material were guaranteed. Additionally, although the mechanical performance did not significantly improve compared to that of regular flattened bamboo sheets, this difference could be attributed to the elimination of certain mechanically significant tissues (such as fiber cells) during the etching process, as

well as the reintroduction of cracks in the cross-section. However, a higher bonding area contributes to greater material stability.

Bio-based composites based on wood and bamboo are widely utilized in building, furniture, transportation, etc. In terms of processing, the innovative grooving and flattening unit eliminates the need for softening in traditional bamboo flattening, integrating standardization and flattening and thereby providing greater economic value. The average production of 1 cubic meter of board saved 65 kg of PF resin adhesive relative to that of bamboo scrimber. In comparison to bamboo composites, this new type of bamboo–wood laminated material has more than twice the efficiency of usage and similar adhesive requirements and needs only half as much bamboo material to produce an average of 1 m$^3$ of board [31]. Overall, the grooving structure does not have a significant impact on the mechanical properties of bamboo laminate materials. The bamboo square composite material can reach the level of conventional bamboo square composites and can be partially replaced. Furthermore, compared to the bamboo composites made by the planing unit, the bamboo composites prepared by the grooving unit may achieve a more dimensional design and are suited to more usage situations with larger size specifications. As a result, the bamboo/wood composite based on the GFB unit in this study may augment and replace existing indoor bamboo–wood composite materials and has a wide range of applications.

**5. Conclusions**

This work successfully developed a novel bamboo–wood composite material using flattened and grooved bamboo units prepared by an efficient integrated machining process. Response surface methodology was applied to model the effects of hot-pressing parameters on the mechanical and bonding performance. Optimization of the parameters produced composites with an excellent MOR and MOE. Furthermore, the physical and chemical bonding mechanisms of the optimized samples were also studied. The following conclusions can be drawn:

Based on the RSM, the optimal hot-pressing process parameters were determined to be 1.18 min/mm hot-pressing time, 1.47 MPa pressure, and a 150 °C temperature. Under these conditions, the bamboo–wood composite exhibited a 121.51 MPa modulus of rupture and an 11.85 GPa modulus of elasticity, which represented only a ~5% error between the experimental and model predictions.

Finite element analysis revealed that, in comparison to homogeneous flat bamboo composites, grooved bamboo composites exhibit distinct tensile ductility and toughness.

Grooving treatment not only effectively improved the wettability of the bamboo surface and increased the permeability of the adhesive on the bamboo surface, but also augmented the bonding area.

## References

1. Hong, C.; Li, H.; Xiong, Z.; Lorenzo, R.; Corbi, I.; Corbi, O.; Wei, D.; Yuan, C.; Yang, D.; Zhang, H. Review of connections for engineered bamboo structures. *J. Build. Eng.* **2020**, *30*, 101324. [CrossRef]
2. Hailemariam, E.K.; Hailemariam, L.M.; Amede, E.A.; Nuramo, D.A. Identification of barriers, benefits and opportunities of using bamboo materials for structural purposes. *Eng. Constr. Archit. Manag.* **2023**, *30*, 2716–2738. [CrossRef]
3. Chen, J.; Guagliano, M.; Shi, M.; Jiang, X.; Zhou, H. A comprehensive overview of bamboo scrimber and its new development in China. *Eur. J. Wood Wood Prod.* **2021**, *79*, 363–379. [CrossRef]
4. Bala, A.; Gupta, S. Engineered bamboo and bamboo-reinforced concrete elements as sustainable building materials: A review. *Constr. Build. Mater.* **2023**, *394*, 132116. [CrossRef]
5. Khajouei-Nezhad, M.; Semple, K.; Nasir, V.; Marggraf, G.; Hauptman, J.; Dai, C. Advances in engineered bamboo processing: Material conversion and structure. *Adv. Bamboo Sci.* **2023**, *5*, 100045. [CrossRef]
6. Wang, J.; Shi, D.; Zhou, C.; Zhang, Q.; Li, Z.; Marmo, F.; Demartino, C. An active-bending sheltered pathway based on bamboo strips for indoor temporary applications: Design and construction. *Eng. Struct.* **2024**, *307*, 117863. [CrossRef]
7. Huang, Y.; Qi, Y.; Zhang, Y.; Yu, W. Progress of bamboo recombination technology in China. *Adv. Polym. Technol.* **2019**, *2019*, 2723191. [CrossRef]
8. Huang, Y.; Ji, Y.; Yu, W. Development of bamboo scrimber: A literature review. *J. Wood Sci.* **2019**, *65*, 25. [CrossRef]
9. Lou, Z.; Li, Y.; Zhao, Y. Bamboo Flattening Technique. In *Bamboo and Sustainable Construction*; Springer: Berlin/Heidelberg, Germany, 2023; pp. 185–210.
10. Chen, L.; Luo, X.; Huang, B.; Ma, Y.; Fang, C.; Liu, H.; Fei, B. Properties and bonding interface characteristics of an innovative bamboo flattening and grooving unit (BFGU) for laminated bamboo lumber. *Colloids Surf. A Physicochem. Eng. Asp.* **2023**, *676*, 132185. [CrossRef]
11. Liu, Y.; Zhou, J.; Fu, W.; Zhang, B.; Chang, F.; Jiang, P. Study on the effect of cutting parameters on bamboo surface quality using response surface methodology. *Measurement* **2021**, *174*, 109002. [CrossRef]
12. Adamu, M.; Rahman, M.R.; Bakri, M.K.B.; Md Yusof, F.A.B.; Khan, A. Characterization and optimization of mechanical properties of bamboo/nanoclay/polyvinyl alcohol/styrene nanocomposites using response surface methodology. *J. Vinyl Addit. Technol.* **2021**, *27*, 147–160. [CrossRef]
13. Chen, L.; Yuan, J.; Wang, X.; Huang, B.; Ma, X.; Fang, C.; Zhang, X.; Sun, F.; Fei, B. Fine gluing of bamboo skin and bamboo pith ring based on sanding. *Ind. Crops Prod.* **2022**, *188*, 115555. [CrossRef]
14. *GB/T17657-2013*; Test Methods of Evaluating the Properties of Wood-Based Panels and Surface Decorated Wood-Based Panels. National Standards of the People's Republic of China: Beijing, China, 2013.
15. Uzcategui, M.G.; Franca, F.J.; Seale, R.D.; Senalik, C.A.; Ross, R.J. Flexural and tensile properties of 2 × 6 and 2 × 10 southern pine lumber: Southenr pine lumber properties. *Wood Fiber Sci.* **2022**, *54*, 257–269. [CrossRef]
16. Baltic, S.; Magnien, J.; Gänser, H.P.; Antretter, T.; Hammer, R. Coupled damage variable based on fracture locus: Prediction of ductile failure in a complex structure. *Int. J. Solids Struct.* **2020**, *207*, 132–144. [CrossRef]
17. Das, A.; Mohanty, K. Optimization of lignin extraction from bamboo by ultrasound-assisted organosolv pretreatment. *Bioresour. Technol.* **2023**, *376*, 128884. [CrossRef] [PubMed]
18. Nkeuwa, W.N.; Zhang, J.; Semple, K.E.; Chen, M.; Xia, Y.; Dai, C. Bamboo-based composites: A review on fundamentals and processes of bamboo bonding. *Compos. Part B Eng.* **2022**, *235*, 109776. [CrossRef]
19. Veza, I.; Spraggon, M.; Fattah, I.R.; Idris, M. Response surface methodology (RSM) for optimizing engine performance and emissions fueled with biofuel: Review of RSM for sustainability energy transition. *Results Eng.* **2023**, *18*, 101213. [CrossRef]
20. Garg, S.; Nayyar, A.; Buradi, A.; Shadangi, K.P.; Sharma, P.; Bora, B.J.; Jain, A.; Shah, M.A. A novel investigation using thermal modeling and optimization of waste pyrolysis reactor using finite element analysis and response surface methodology. *Sci. Rep.* **2023**, *13*, 10931. [CrossRef] [PubMed]
21. Mo, T.; Chen, Z.; Zhou, D.; Lu, G.; Huang, Y.; Liu, Q. Effect of lamellar structural parameters on the bending fracture behavior of AA1100/AA7075 laminated metal composites. *J. Mater. Sci. Technol.* **2022**, *99*, 28–38. [CrossRef]
22. Shi, J.; Liang, Y.; Yu, H.; Ban, Z.; Zhang, Y.; Yang, W.; Yu, W. A new strategy for bamboo ultra-long radial slice preparation and novel composite fabrication. *Ind. Crops Prod.* **2023**, *203*, 117232. [CrossRef]
23. Wang, X.; Yao, Y.; Xie, X.; Yuan, Z.; Li, W.; Yuan, T.; Huang, Y.; Li, Y. Investigation of the microstructure, chemical structure, and bonding interfacial properties of thermal-treated bamboo. *Int. J. Adhes. Adhes.* **2023**, *125*, 103400. [CrossRef]
24. Su, H.; Du, G.; Ren, X.; Liu, C.; Wu, Y.; Zhang, H.; Ni, K.; Yin, C.; Yang, H.; Ran, X. High-performance bamboo composites based on the chemical bonding of active bamboo interface and chitosan. *Int. J. Biol. Macromol.* **2023**, *244*, 125345. [CrossRef] [PubMed]
25. Zhou, H.; Wei, X.; Smith, L.M.; Wang, G.; Chen, F. Evaluation of uniformity of bamboo bundle veneer and bamboo bundle laminated veneer lumber (BLVL). *Forests* **2019**, *10*, 921. [CrossRef]
26. Zhang, J.; Ren, H.; Zhong, Y.; Zhao, R. Analysis of compressive and tensile mechanical properties of recombinant bamboo. *J. Nanjing For. Univ.* **2012**, *36*, 107–111.
27. Han, J.; Gao, X.T. A study on tensile mechanical properties of bamboo plywood. *Adv. Mater. Res.* **2011**, *291*, 1009–1014. [CrossRef]
28. Qi, J.Q.; Xie, J.L.; Huang, X.Y.; Yu, W.J.; Chen, S.M. Influence of characteristic inhomogeneity of bamboo culm on mechanical properties of bamboo plywood: Effect of culm height. *J. Wood Sci.* **2014**, *60*, 396–402. [CrossRef]

29. Chen, G.; Yu, Y.; Li, X.; He, B. Mechanical behavior of laminated bamboo lumber for structural application: An experimental investigation. *Eur. J. Wood Wood Prod.* **2020**, *78*, 53–63. [CrossRef]
30. Jain, S.; Kumar, R.; Jindal, U. Mechanical behaviour of bamboo and bamboo composite. *J. Mater. Sci.* **1992**, *27*, 4598–4604.
31. Lou, Z.; Zheng, Z.; Yan, N.; Jiang, X.; Zhang, X.; Chen, S.; Xu, R.; Liu, C.; Xu, L. Modification and Application of Bamboo-Based Materials: A Review—Part II: Application of Bamboo-Based Materials. *Forests* **2023**, *14*, 2266. [CrossRef]